PERGAMON

International Journal of Solids and Structures 37 (2000) 5447–5464

INTERNATIONAL JOURNAL OF SOLIDS and STRUCTURES

www.elsevier.com/locate/ijsolstr

A comprehensive unit cell model: a study of coupled effects in piezoelectric 1–3 composites

Heinz E. Pettermann [1], Subra Suresh*

Department of Materials Science and Engineering, Massachusetts Institute of Technology, Cambridge, MA 02139, USA

Received 24 May 1998; in revised form 17 August 1999

Abstract

A finite element unit cell model for investigation of arbitrary loading conditions is developed for composites with periodic arrangements of continuous aligned fibers. Special emphasis is placed on the formulation of the boundary conditions to allow for simulation of all modes of overall deformation arising from any arbitrary combination of mechanical and electrical loading. The model is applied to piezoelectric composites whereby the overall elastic, dielectric, as well as piezoelectric moduli are fully extracted. The boundary conditions are validated for elastic in-plane shear loading and checked by recourse to comparisons with analytical bounds as well as semianalytical bounds and experimental investigations for piezoelectric composites from the literature. Aspects of fiber arrangement and differences between piezoelectric ceramic as well as polymer matrix composites reinforced with piezoelectric fibers are discussed. © 2000 Published by Elsevier Science Ltd.

Keywords: Boundary conditions; Composite materials; Fiber reinforced; Finite element; Homogenization; Micro mechanics; Modeling; Piezoelastic

1. Introduction

Piezoelectric materials have been successfully used in the past decades as transducers, sensors, and micro-actuators. Fibrous composites show lower mechanical losses than monolithic materials. They are also candidate materials for use as sensors to assess the structural integrity and damage tolerance of load-bearing structures such as airplane wings. For such applications, the materials are typically loaded within the linear regime. It is of interest to know the overall coupled electro-mechanical behavior and the local fields in the constituent phases, as well as the response under complex loading conditions.

* Corresponding author. Tel.: +1-617-253-3320; fax: +1-617-253-0868.
E-mail address: ssuresh@mit.edu (S. Suresh).
[1] Present address: Division of Materials Technology, Austrian Research Centers, A-2444 Seibersdorf, Austria

0020-7683/00/$ - see front matter © 2000 Published by Elsevier Science Ltd.
PII: S0020-7683(99)00224-3

A number of methods have been developed to predict and simulate the linear coupled piezoelectric and mechanical behavior of composites. Basic analytical approaches have been reported, e.g. Chan and Unsworth, 1989; Smith and Auld, 1991, which are not capable of predicting the response to general loading, i.e. they do not give the full set of overall moduli. Semianalytical and Hashin/Shtrikman-type bounds for describing the complete overall behavior (i.e. all elements of the material tensors) have been developed (Bisegna and Luciano, 1996, 1997) which are useful tools for theoretical considerations. However, the range between the bounds can be very wide for certain overall (i.e. bulk) moduli. Mechanical mean field type methods have been extended to include electroelastic effects (Benveniste, 1993; Dunn and Taya, 1993; Wang, 1992; Chen, 1993) based on an Eshelby-type solution for a single inclusion in an infinite matrix (Benveniste, 1992; Dunn and Wienecke, 1997). Such mean field type methods are capable of predicting the entire behavior under arbitrary loads. However, they use averaged representations of the electrical and mechanical fields within the constituents of the composite, i.e. they do not account for the local fluctuations in field quantities. This restriction can be overcome by employing periodic microfield approaches (commonly referred to as unit cell models) where the fields are typically solved numerically with high resolution, e.g. by the finite element method (Gaudenzi, 1997). In such models the representative unit cell and the boundary conditions are designed to capture a few special load cases which are connected to specific deformation patterns (e.g. Brockenbrough and Suresh, 1990; Böhm, 1993; Gunawardena et al., 1993; Cleveringa et al., 1997). This allows the prediction of only a few of the key material parameters; for example, only normal loads can be applied consistently using the symmetry boundary conditions.

To the knowledge of the authors, the only unit cell models which capture the entire behavior correctly so far have been reported by Teply and Dvorak (1988) and recently by Smit et al. (1998). Presumbly correct boundary conditions are employed in Reisner et al. (1998), Bisegna and Luciano (1997), although no details are given. A different method which can handle arbitrary loading scenarios is the so called *asymptotic homogenization approach* (Suquet, 1987). For two-dimensional cases within the context of masonry the set of boundary conditions is given by Anthoine (1995) and Luciano and Sacco (1997).

The aim of this paper is to account for local fluctuations of the fields and to predict the full set of material moduli, i.e. to determine the complete tensors associated with the overall elastic, dielectric and piezoelectric behavior. This means that the linear response to any mechanical and electrical load, or any combination of both, will be determined. Such a comprehensive finite element unit cell model is developed and the coupled linear piezoelectric and elastic behavior of unidirectional continuous fiber composites is investigated. Periodic hexagonal and square fiber arrangements (see e.g. Brockenbrough and Suresh, 1990; Böhm, 1993) are examined for piezoelectric fibers belonging to the $6/mm$ crystal class (see e.g. Nye, 1957; IEEE, 1978). The sixfold axes (in terms of crystal symmetry) are the longitudinal axes of the fibers embedded in a dielectric matrix material. The finite element code (ABAQUS, 1996) is used, which is based on a displacement/electric potential formulation and provides an option for linear fully coupled piezoelectric material behavior. Once the entire behavior is determined, further parameters used for characterization, such as the coupling factors (IEEE, 1978), can be calculated because they are directly related to the moduli.

The validity of the comprehensive unit cell model is proven by predicting the in-plane shear response of a transversally isotropic elastic composite using two different load scenarios: one relying on the comprehensive boundary conditions, the other modeling simple shear by employing standard symmetry boundary conditions. Aspects of fiber arrangements are discussed. The differences between piezoelectric composites and monolithic materials as well as poled and unpoled fiber materials are addressed. Theoretical bounds and experimentally evaluated material data reported in the literature on the overall behavior are compared with the results of the present approach.

It is noted that the approach introduced in this work is not limited specifically to piezoelectric problems, but can be applied to unit cell investigations in general, e.g. for thermo-elasto-plastic

simulations. In addition to the homogenization procedure (extracting the overall behavior), localization can be performed with high accuracy, i.e. the local inhomogeneous fields can be obtained for an arbitrary overall load. This means the present model is suited for generating the input necessary for Dvorak's Transformation Field Analysis (Dvorak, 1992), in which information on the interrelation between overall and local behavior is required. The procedures presented in the current paper can also be applied to more complex unit cells with periodic boundary conditions, such as the random microstructures considered in Nakamura and Suresh (1993) or Moulinec and Suquet (1994).

2. Constitutive equations

2.1. General relations and notation

In a piezoelectric material, the elastic and the dielectric responses are coupled. The coupled linear constitutive equations can be given in tensor notation as,

$$\begin{aligned} \sigma_{ij} &= C^E_{ijkl}\varepsilon_{kl} - e_{ijk}E_k \\ D_i &= e_{ikl}\varepsilon_{kl} + \kappa^{\varepsilon}_{ij}E_j \end{aligned}, \tag{1}$$

where σ_{ij} and ε_{kl} are the second rank stress and strain tensors, respectively. D_i and E_j denote the vectors of the electric flux density (or electric displacement) and the electric field (or field strength), respectively. The latter is the negative gradient of the electric potential, $E_i = -\partial\phi/\partial x_i$. In the case of coupled material laws, the moduli must be given under specified conditions, such as C^E_{ijkl} denoting the fourth rank elasticity tensor for zero electric field, and $\kappa^{\varepsilon}_{ij}$ denoting the second rank tensor of the electric permeabilities for zero strain; finally e_{ijk} is the appropriate third rank piezoelectric coupling tensor.

Instead of the above tensor notation, matrix notation (see e.g. Nye, 1957) can be employed to represent Eq. (1) as,

$$\begin{pmatrix} \boldsymbol{\sigma} \\ \boldsymbol{D} \end{pmatrix} = \begin{pmatrix} \boldsymbol{C}^E & -\boldsymbol{e}^{\mathrm{T}} \\ \boldsymbol{e} & \boldsymbol{k}^{\varepsilon} \end{pmatrix} \begin{pmatrix} \boldsymbol{\varepsilon} \\ \boldsymbol{E} \end{pmatrix}, \tag{2}$$

where the stress and strain tensors are represented by the vectors of their components,

$$\boldsymbol{\sigma} = \begin{pmatrix} \sigma_{11} \\ \sigma_{22} \\ \sigma_{33} \\ \sigma_{23} \\ \sigma_{13} \\ \sigma_{12} \end{pmatrix}, \quad \boldsymbol{\varepsilon} = \begin{pmatrix} \varepsilon_{11} \\ \varepsilon_{22} \\ \varepsilon_{33} \\ 2\varepsilon_{23} \\ 2\varepsilon_{13} \\ 2\varepsilon_{12} \end{pmatrix}. \tag{3}$$

The vectors and tensors, respectively, of $\boldsymbol{E}$, $\boldsymbol{D}$, and $\boldsymbol{\kappa}^{\varepsilon}$ remain unchanged with respect to Eq. (1). The matrix of piezoelectric moduli is composed from the tensor elements as,

$$\boldsymbol{e} = \begin{pmatrix} e_{111} & e_{122} & e_{133} & e_{123} & e_{113} & e_{112} \\ e_{211} & e_{222} & e_{233} & e_{223} & e_{213} & e_{212} \\ e_{311} & e_{322} & e_{333} & e_{323} & e_{313} & e_{312} \end{pmatrix}, \tag{4}$$

and the elements of the elasticity matrix are

$$\boldsymbol{C}^E_{ab} = C^E_{ijkl}, \tag{5}$$

where the subscripts a and b, respectively, are deduced from ij and kl, respectively, as $11 \rightarrow 1$, $22 \rightarrow 2$, $33 \rightarrow 3$, $23 \rightarrow 4$, $13 \rightarrow 5$, $12 \rightarrow 6$; and the symmetries $ab = ba$, $ij = ji$, $kl = lk$ hold.

The superscript T denotes the transpose of a matrix. In the most general case there exist 21 elastic, 6 dielectric, and 18 piezoelectric material constants which are mutually independent.

In the previous equations the stresses are combined with the electric flux density and the strains with the electric field, respectively. There is no restriction to this particular assignment; in fact, for other applications the following set of equations might be of advantage;

$$\begin{pmatrix} \boldsymbol{\sigma} \\ \boldsymbol{E} \end{pmatrix} = \begin{pmatrix} \boldsymbol{C}^{D} & -\boldsymbol{h}^{\mathrm{T}} \\ -\boldsymbol{h} & \boldsymbol{\beta}^{\varepsilon} \end{pmatrix} \begin{pmatrix} \boldsymbol{\varepsilon} \\ \boldsymbol{D} \end{pmatrix}, \tag{6}$$

where $\boldsymbol{C}^{\mathrm{D}}$ is the elasticity matrix for zero electric displacement, $\boldsymbol{\beta}^{\varepsilon}$ is the inverse of the permeability tensor for zero strain in Eq. (2), and $\boldsymbol{h}$ is the appropriate piezoelectric coupling matrix. Equivalent relations as given in Eqs. (4) and (5) hold for $\boldsymbol{C}^{\mathrm{D}}$ and $\boldsymbol{h}$, respectively.

Two more sets of equations are given by the inverse relations of Eqs. (2) and (6), respectively. However, a simple matrix inversion of the 9×9 matrices containing the material moduli is not possible, since these composed matrices do not represent tensors. There exist a number of relations between the various tensors and their elements which are given in the literature. Also the relations equivalent to Eqs. (4) and (5) appear in a modified version (where selected elements are multiplied by factors), see e.g. IEEE, 1978.

In general, elastic dielectric material behavior can be obtained by setting the piezoelectric moduli $\boldsymbol{e} = \boldsymbol{h} = \boldsymbol{0}$, i.e. removing the coupling, see Eqs. (1), (2) and (6).

It is noted that the finite element program, ABAQUS (1996), relies on Eqs. (1) and (2) because it is based on a displacement formulation. This point and the following section serve as the basis for discussion of the applications given below, as elaborated in greater detail in subsequent discussion.

2.2. Restriction to certain crystal classes

In the present work constituent materials and composites are considered both of which can be described by the constitutive equations of *6 and 4/mm* crystals[1], respectively (see e.g. Nye, 1957; IEEE, 1978). Six mm crystals show a transversally isotropic behavior and a rotation with respect to their poling axis alters neither their mechanical nor electrical response. For *4/mm* crystals this holds true for the piezoelectric and dielectric behavior but not for the elastic behavior.

Letting the poling axes coincide with direction 3 the expanded notation of Eq. (6) for a *4/mm* crystal reads

$$\begin{pmatrix} \sigma_{11} \\ \sigma_{22} \\ \sigma_{33} \\ \sigma_{23} \\ \sigma_{13} \\ \sigma_{12} \\ E_1 \\ E_2 \\ E_3 \end{pmatrix} = \begin{pmatrix} \boldsymbol{C}^{D}_{11} & \boldsymbol{C}^{D}_{12} & \boldsymbol{C}^{D}_{13} & \cdot & \cdot & \cdot & \cdot & \cdot & -\boldsymbol{h}_{31} \\ \boldsymbol{C}^{D}_{12} & \boldsymbol{C}^{D}_{11} & \boldsymbol{C}^{D}_{13} & \cdot & \cdot & \cdot & \cdot & \cdot & -\boldsymbol{h}_{31} \\ \boldsymbol{C}^{D}_{13} & \boldsymbol{C}^{D}_{13} & \boldsymbol{C}^{D}_{33} & \cdot & \cdot & \cdot & \cdot & \cdot & -\boldsymbol{h}_{33} \\ \cdot & \cdot & \cdot & \boldsymbol{C}^{D}_{44} & \cdot & \cdot & \cdot & -\boldsymbol{h}_{51} & \cdot \\ \cdot & \cdot & \cdot & \cdot & \boldsymbol{C}^{D}_{44} & \cdot & -\boldsymbol{h}_{51} & \cdot & \cdot \\ \cdot & \cdot & \cdot & \cdot & \cdot & \boldsymbol{C}^{D}_{66} & \cdot & \cdot & \cdot \\ \cdot & \cdot & \cdot & \cdot & -\boldsymbol{h}_{51} & \cdot & \boldsymbol{\beta}^{\varepsilon}_{11} & \cdot & \cdot \\ \cdot & \cdot & \cdot & -\boldsymbol{h}_{51} & \cdot & \cdot & \cdot & \boldsymbol{\beta}^{\varepsilon}_{11} & \cdot \\ -\boldsymbol{h}_{31} & -\boldsymbol{h}_{31} & -\boldsymbol{h}_{33} & \cdot & \cdot & \cdot & \cdot & \cdot & \boldsymbol{\beta}^{\varepsilon}_{33} \end{pmatrix} \begin{pmatrix} \varepsilon_{11} \\ \varepsilon_{22} \\ \varepsilon_{33} \\ 2\varepsilon_{23} \\ 2\varepsilon_{13} \\ 2\varepsilon_{12} \\ D_1 \\ D_2 \\ D_3 \end{pmatrix}, \tag{7}$$

[1] Due to the nature of piezoelectricity which requires a perovskite structure (i.e. the lack of a center of symmetry), these two crystal classes are those with the highest degree of symmetry, in which this phenomenon can occur (Nye, 1957).

where the number of independent moduli compared to the most general case reduces from 21 to 6 elastic, from 6 to 2 dielectric, and from 18 to 3 piezoelectric parameters; note the multiple appearance of some elements.

For *6/mm* crystals, the in-plane shear modulus is a function of the in-plane Young's modulus and Poisson ratio. In terms of Eq. (7) this reads,

$$\boldsymbol{C}^D_{66} = \frac{\boldsymbol{C}^D_{11} - \boldsymbol{C}^D_{12}}{2}, \tag{8}$$

and the number of mutually independent elastic moduli is further reduced to 5. The number of dielectric and piezoelectric moduli remains unchanged.

2.2.1. Material symmetry of the composites

This work is focused on piezoelectric fibers belonging to the crystal class *6/mm*, such as $BaTiO_3$ and PZT. The fiber properties are invariant with respect to rotation about their longitudinal axis (the poling axis) and corresponding orientations of the fibers have no influence on the overall symmetry and behavior of the composite. It should be noted that this would not hold true for fibers belonging to the *4/mm* crystal class.

In an analogous way to the behavior of crystals, the overall behavior of inhomogeneous materials is strongly determined by their overall symmetry, which can be described by the same formalism. For a regular hexagonal arrangement of the fibers (which has a six-fold axis of symmetry with respect to the fiber direction) a transversally isotropic composite results, to be described by the constitutive equation of a *6/mm* crystal. A regular square arrangement (with a four-fold symmetry axis) gives rise to a tetragonal behavior, to be described by the constitutive equation of a *4/mm* crystal.

3. The comprehensive unit cell model

The aim of this section is to present a comprehensive unit cell model which is capable of predicting the complete set of material moduli for continuous fiber reinforced composites with periodic microstructures. This requires an extension of the standard unit cell models used for investigating such classes of composites.

Within the context of displacement formulated finite element approaches the mechanical degrees of freedom are the three displacement components; the electrical degree of freedom is the electric potential. Their derivatives with respect to the spatial coordinates are the strains and the negative electric field, respectively. Thus, the formulation of the constitutive behavior as given in Eqs. (1) and (2) is well suited for displacement oriented finite element methods. It is noted that commercially available finite element software, i.e. ABAQUS (1996), is used which is based on a strain energy approach; the complementary approach is not considered within the present paper. Once the mechanical boundary conditions are known, the introduction of the electric boundary conditions is straightforward because they follow the same rules but on a level which is one degree less complex.

For modeling continuous fiber composites, *generalized plane strain*[2] models are typically employed which is an extensively used and widely accepted approach (see, e.g., Brockenbrough and Suresh, 1990; Böhm, 1993). A periodic arrangement of fibers can be represented by a rectangular unit cell showing

[2] Here, generalized plane strain means that the normal strain in the direction perpendicular to the modeling plane is constant throughout the model.

two quarters of the fiber cross section at opposite corners and using symmetry boundary conditions (i.e. forcing the boundaries to remain straight and parallel to its initial configuration). Modifying the dimensions of the unit cell and the boundary conditions, different (periodic) fiber arrangements have been investigated such as clustered and distorted topologies (Böhm and Rammerstorfer, 1995). In addition, unit cells with up to 60 randomly located fibers (Nakamura and Suresh, 1993) also combined with periodic boundary conditions (Moulinec and Suquet, 1994) have been reported. However, such models are restricted to certain loading conditions.

One of the objectives of this work was to overcome the restrictions to specific load cases by introducing an extended (rectangular) unit cell model. To enable the modeling of shear deformation in the plane transverse to the fibers the representative volume element and the boundary conditions must be chosen with care. It will be shown later that a certain design of the unit cell is required which is different from the standard models. Since the deformations along a boundary between two corners are not known a priori (except for some special load cases), the boundary conditions must allow for the adjustment to the deformation in an appropriate manner. Special care must been taken to avoid over- or under-constraining. It is noted, that a uniform displacement along the boundary (according to shear strain in a homogeneous material) as used by Cleveringa et al. (1997) is not proper under general loading conditions for a composite.

3.1. Representative unit cell

Fig. 1 shows a regular hexagonal arrangement of continuous fibers embedded in a matrix. An element which captures the total geometric information is indicated by the solid line. Note that this element shows a center of symmetry with respect to the middle fiber. If this element is repeated periodically in the horizontal and vertical directions (that is by translation), the infinite repeating fiber pattern can be reproduced. For general loading conditions periodic boundary conditions (to be introduced below) must be used to describe the displacements and the electric field. The same information is obviously captured by the element outlined with the long dashed line (Fig. 1). This invariance with respect to translations allows the representative element to be reduced by 50% without loss of information. Thus, the unit cell as used in the present work is obtained as given by the dotted perimeter.

By changing the horizontal or vertical spacing between the fibers periodic hexagonal arrangements and square arrangements in diagonal orientation can be realized; compare the unit cells for hexagonal

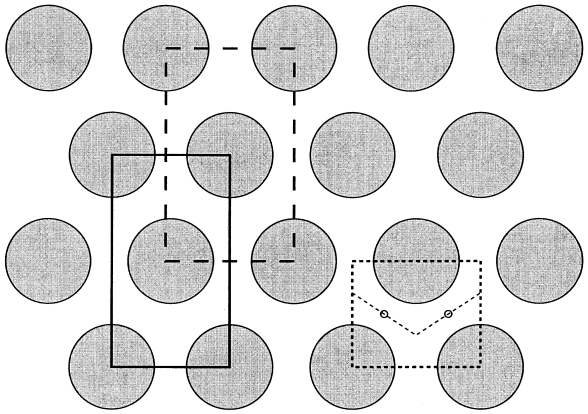

Fig. 1. Cross section of a periodic hexagonal fiber arrangement; basic cell of periodicity (solid and long dashed line) and the present unit cell (dotted line).

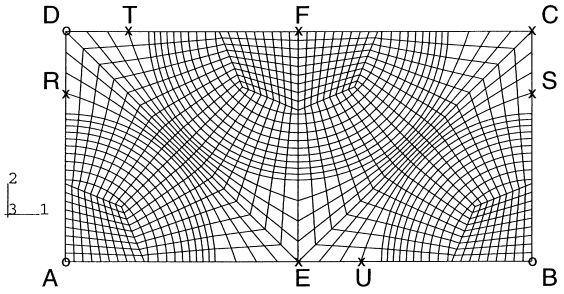

Fig. 2. Bottom view of the unit cell for the periodic square arrangement designed for modeling fiber volume fractions from 20 to 65% with 5% resolution; master nodes (○) for controlling the deformation and auxiliary nodes (×) used in the text for describing the boundary conditions.

arrangements in Fig. 1 (dotted) and for square arrangements in Fig. 2 (note the difference in the aspect ratio of the unit cells). The latter contains implicitly the behavior of the square arrangement in edge orientation. Since the material tensors will be known completely when employing the present model, a coordinate transformation can be performed. In addition, fiber arrangements of adjustable "skewness" can be realized by changing the aspect ratio of the unit cell.

3.2. Boundary conditions

The finite element discretization of the square arrangement is shown in Fig. 2. The boundary conditions apply for this as well as for the hexagonal unit cell model. Throughout the present work isoparametric finite elements with linear interpolation functions are used. The nodes indicated by circles are the "master nodes" which control the overall behavior of the model. In all other nodal displacements at the boundaries the appropriate conditions of periodicity must be incorporated and be linked to the master nodes in terms of equations. The degrees of freedom along the vertical sides are connected by periodic boundary conditions, i.e. the shape of both sides must match each other exactly. For the nodes R and S in Fig. 2 this reads in terms of the master nodes A and B,

$$u^R - u^A = u^S - u^B, \tag{9}$$

where u stands for any of the degrees of freedom, i.e. u_1, u_2 and u_3 for the displacements as well as ϕ for the electric potential. Using the node A as the fixed node (i.e. $u^A = 0$) gives rise to,

$$u^S - u^B - u^R = 0. \tag{10}$$

For the horizontal boundary the invariance with respect to translation is utilized. The degrees of freedom at the upper left half (e.g. for the node T) are expressed in terms of the lower right part (node U) and the master nodes as,

$$u^T - u^D = u^U - u^E \quad \text{or} \quad u^T - u^D - u^U + u^E = 0, \tag{11}$$

where the degree of freedom of node E follows from the central symmetry of the large volume element in Fig. 1 as,

$$u^E = \frac{u^B - u^A}{2}. \tag{12}$$

Equivalent relations can be given for relating the upper right to the lower left part, and for the node F.

Out-of-plane shear deformation (shear in the fiber direction) can be introduced either by a more general formulation of the strain state at the level of the finite element definition (Adams and Crane, 1984) or by using a 3D model employing appropriate boundary conditions. The latter approach is adopted in the present work, where instead of the 2D model a "slice model" is used whose thickness in fiber direction is just one element. Thus, Fig. 2 actually shows the "bottom plane" of the 3D model. Another master node at the top plane, $\bar{A}$ (not shown), is defined with the same x_1 and x_2 coordinates as node A, which controls the normal strain in fiber direction. All other nodes on the top plane are connected to their counterparts on the bottom plane by appropriate equations. The out-of-plane displacement and the electric potential for any pair of nodes Y and $\bar{Y}$ follow a periodicity condition,

$$u^Y - u^{\bar{Y}} = u^A - u^{\bar{A}} \quad \text{for } u = u_3, \phi, \tag{13}$$

and the in-plane deformations for all nodes including $\bar{A}$ read,

$$u^{\bar{Y}} = u^Y \quad \text{for } u = u_2, u_3. \tag{14}$$

It is noted again that Eqs. (9)–(12) are also valid for the out-of-plane deformations along the boundaries.

The out-of-plane strain in general reads as,

$$2\varepsilon_{i3} = \frac{\partial u_3}{\partial x_i} + \frac{\partial u_i}{\partial x_3} \quad \text{with } i = 1, 2 \tag{15}$$

The boundary conditions as chosen in Eqs. (13) and (14) imply that $\frac{\partial u_i}{\partial x_3} = 0$ without loss of generality.

At the master nodes deformations can be prescribed according to the homogeneous overall strains and the reaction forces acting on these nodes may be related to overall stresses by the unit cell cross sections or vice versa. Local stress fluctuations at the boundaries are self equilibrated because of the boundary conditions and do not contribute to the overall stress.

Symmetry boundary conditions often employed to simulate uniaxial loading are implicitly contained in the present model as a simpler subset.

The scalar valued electric potential follow the same conditions, even more since the degree of complexity is reduced by one order compared to the vector valued displacements. The validity of the present boundary conditions is discussed in the next section. It is noted that periodic boundary conditions are applicable for any cell providing compatibility of the corresponding faces.

4. Applications and discussion

The comprehensive unit cell model is applied to purely elastic as well as piezoelectric composites. Various investigations are performed in order to assess the validity of the model. Comparisons to theoretical bounds and experimental results from the literature for the effective piezoelastic behavior are carried out.

Table 1
Material data for the piezoelectric fibers (PZT-7A) and the dielectric matrix (epoxy) after Bisegna and Luciano (1997)

	PZT-7A	Epoxy
$\mathbf{C}^E_{11}$ (GPa)	154.837	8.0
$\mathbf{C}^E_{33}$ (GPa)	131.39	8.0
$\mathbf{C}^E_{12}$ (GPa)	83.237	4.4
$\mathbf{C}^E_{13}$ (GPa)	82.712	4.4
$\mathbf{C}^E_{44}$ (GPa)	25.696	1.8
$\mathbf{C}^E_{66}$ (GPa)	35.800	1.8
$\boldsymbol{\kappa}^\varepsilon_{11}$ (nC/Vm)	4.065	0.0372
$\boldsymbol{\kappa}^\varepsilon_{33}$ (nC/Vm)	2.079	0.0372
$\boldsymbol{e}_{31}$ (C/m^2)	−2.120582	–
$\boldsymbol{e}_{33}$ (C/m^2)	9.521830	–
$\boldsymbol{e}_{51}$ (C/m^2)	9.349593	–

4.1. Elastic composites

4.1.1. Comparison to bounds

At first the purely elastic behavior is investigated and the overall moduli resulting from the present model are compared to the analytical Hashin/Shtrikman (HS) bounds for transversally isotropic materials (Hashin, 1983). The constituent material data from Bisegna and Luciano (1997) are adopted, see Table 1; the dielectric and the piezoelectric moduli are neglected for the purely elastic considerations. A composite with 40% volume fraction of fibers is investigated for periodic square arrangements in edge (SQE) as well as diagonal (SQD) orientation and hexagonal arrangements (HEX), respectively; the fiber cross section is circular. The predicted overall moduli are listed in Table 2, where, in addition, the upper and lower HS bounds are given.

The hexagonal arrangement gives rise to transversally isotropic overall behavior and can be compared to the HS bounds directly. All moduli predicted by the unit cell fall within these rigorous bounds. The transverse Young's modulus, E_1, is close to the lower bound, which is the typical behavior when the fibers are stiffer than the matrix. The longitudinal Young's modulus, E_3, is in excellent agreement with the bounds which are very tight for this case (the difference is below the displayed accuracy).

The transverse shear modulus, G_{12}, is close to the lower bound and the longitudinal shear modulus, G_{13}, is in agreement with its lower bound. It is noted that of the three transverse moduli, E_1, ν_{12}, and G_{12}, only two are mutually independent for transversally isotropic material behavior.

In addition to the results for the hexagonal arrangement, the values for the square arrangements are displayed in Table 2. The same effective behavior is given with respect to two different coordinate systems, i.e. the axes are oriented along the diagonal directions (SQD) and along the edge directions (SQE), respectively, of the square arrangement morphology. Since the square fiber arrangements do not show transversally isotropic overall material symmetry but have tetragonal symmetry, the results need not comply with these bounds, and the Poisson ratios can be greater than 0.5. For the in-plane moduli (which are now mutually independent) a marked direction-dependence is observed. This behavior depends on whether or not there exist continuous matrix regions which are loaded in such a way that no distinct reinforcing effect can occur in this regions (Moulinec and Suquet, 1994; Böhm and Rammerstorfer, 1995); e.g. under pure in-plane shear along the edge direction there are wide "unreinforced" regions. Under pure shear along the diagonal, however, such regions are markedly narrower (at a given volume fraction) and a stiffer behavior results.

Table 2
Predicted elastic effective Young's moduli, Poisson ratios, and shear moduli for hexagonal (HEX), square diagonal (SQD), and square edge (SQE) fiber arrangements compared to the Hashin/Shtrikman bounds (HS) for 40 vol% of circular fibers

	HEX	SQD	SQE	HS
E_1 (GPa)	10.38	9.39	11.84	10.24/16.79
E_3 (GPa)	32.49	32.49	32.49	32.50/32.50
ν_{12}	0.448	0.502	0.372	–
ν_{13}	0.351	0.352	0.352	–
G_{12} (GPa)	3.85	4.32	3.13	3.51/5.54
G_{13} (GPa)	3.72	3.74	3.74	3.72/8.08

4.1.2. Validation of boundary conditions

The hexagonal arrangement provides a powerful tool for validating the present unit cell approach with respect to the boundary conditions. Since this arrangement shows transversally isotropic behavior the in-plane shear modulus is independent of the orientation within the plane transverse to the fibers. The in-plane shear response can be determined by applying only normal loading such that $\sigma_{11} = -\sigma_{22}$, which corresponds to pure shear in the 45° direction. The resulting strain tensor represents pure shear in that direction and the shear modulus is determined. Alternatively, the capability of the present model is used to simulate pure shear such that σ_{12} is the only non-zero stress component. This yields exactly the same value for the shear modulus and, thus, proves the validity of the present model. Note that the latter procedure requires a consistent formulation of the boundary conditions, in order not to over- or under-constrain the unit cell. Fig. 3 shows the deformation mode where overall pure shear is applied as,

$$2\varepsilon_{12} = \frac{\partial u_1}{\partial x_2} + \frac{\partial u_2}{\partial x_1}. \tag{16}$$

All features with respect to the boundary conditions as described in the previous section can be observed, i.e. the periodicity along the vertical edges and the invariance with respect to translation along the horizontal edges. The applied boundary conditions also become obvious in Fig. 4, where pure shear is applied in fiber direction, $2\varepsilon_{23}$, according to Eq. (15). Note that the top and bottom 1–3 planes and the side 2–3 planes remain plane despite the fact that no such constraints are imposed by the boundary conditions. It is noted that for this special load case the right or the left half of the present unit cell alone would be sufficient.

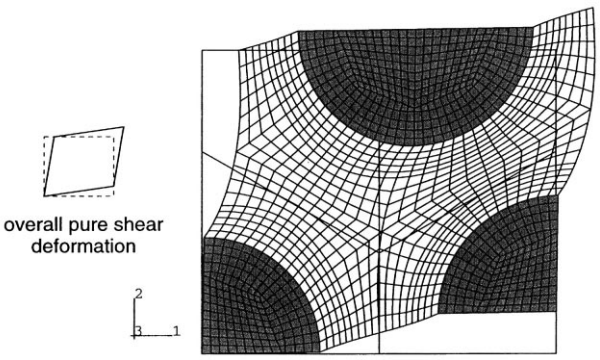

Fig. 3. Predicted deformation of the hexagonal unit cell representing 40 vol% of fibers under overall pure in-plane shear.

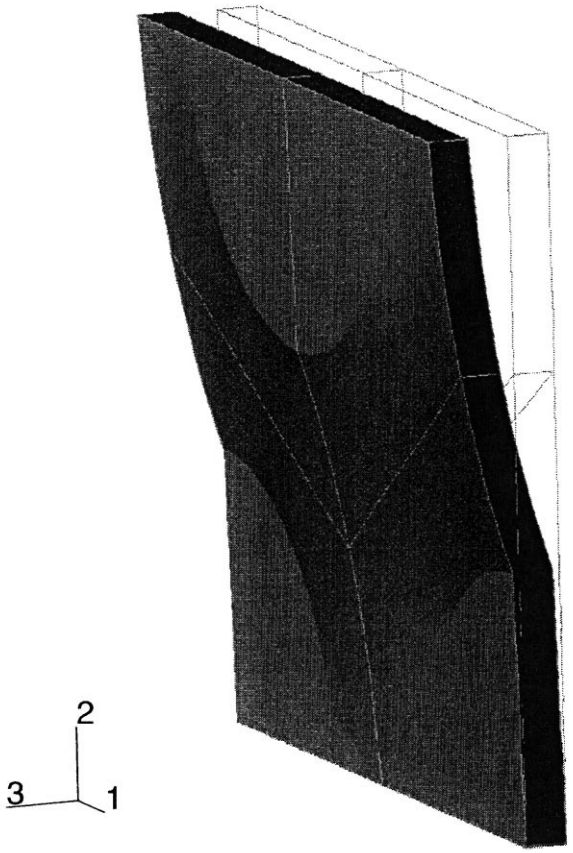

Fig. 4. Predicted deformation of the hexagonal unit cell representing 40 vol% of fibers under overall pure out-of-plane shear.

In both Figs. 3 and 4 the local distribution of the deformations can be observed under transverse and axial shear loading, respectively. It is interesting to note that in both figures central symmetric deformation patterns are exhibited in both the left and the right half of the model. This indicates that the representative unit cell could be reduced again by 50% obtaining the upper or lower pentagonal shapes sketched by the dotted line in Fig. 1 (as well as introducing additional point symmetry boundary conditions and a proper definition of the master nodes). In fact, the inclination of the notch (or "the roof") does not matter as long as the center points of the left and right half (marked with circles in Fig. 1) are part of it. For example, the PHA model by Teply and Dvorak (1988), which comprises a triangular cross section with corners at the fiber centers, is capable of modeling general deformation in a correct manner.

Correct behavior (with respect to all possible modes of deformation) cannot be captured by the left or the right half of the unit cell alone. Note the deformation modes of "barreling" and "inverse barreling", respectively, of both halves in Fig. 3. The interaction between these two halves is necessary to represent the correct behavior (and cannot be modeled by special boundary conditions on one of such halves).

Table 3
Predictions for the complete set of piezoelectric effective properties for hexagonal (HEX), square diagonal (SQD), and square edge (SQE) fiber arrangements for circular ($^{\bigcirc}$) and quadratic ($^{\square}$) fiber cross-sections compared to the tightest bounds available (BL) and Hashin/Shtrikman-type bounds (HS-type) from Bisegna and Luciano (1997) for 60 vol% of fibers

	HEX$^{\bigcirc}$	SQD$^{\bigcirc}$	SQE$^{\bigcirc}$	SQD$^{\square}$	SQE$^{\square}$	BL	HS-type
$\mathbf{C}^D_{11}$ (GPa)	22.41	21.62	25.19	21.05	25.42	25.2/25.5	24.9/28.7
$\mathbf{C}^D_{33}$ (GPa)	86.91	87.10	87.10	86.98	86.98	76.1/87.0	79.0/87.8
$\mathbf{C}^D_{12}$ (GPa)	10.51	12.33	8.76	12.23	7.86	7.72/8.15	5.00/12.0
$\mathbf{C}^D_{13}$ (GPa)	10.53	10.84	10.84	10.64	10.64	8.89/12.3	6.12/16.5
$\mathbf{C}^D_{44}$ (GPa)	6.34	6.70	6.70	6.51	6.51	6.45/6.52	6.40/7.67
$\mathbf{C}^D_{66}$ (GPa)	5.95	8.22	4.64	8.78	4.41	4.39/4.41	4.37/4.92
$\boldsymbol{\beta}^{\varepsilon}_{11}$ (GVm/C)	6.809	6.341	6.341	6.572	6.572	6.57/6.66	2.54/6.73
$\boldsymbol{\beta}^{\varepsilon}_{33}$ (GVm/C)	0.780	0.780	0.780	0.780	0.780	0.730/0.844	0.742/0.951
$\boldsymbol{h}_{31}$ (GV/m)	−0.150	−0.157	−0.157	−0.153	−0.153	−0.337/0.024	−1.03/0.719
$\boldsymbol{h}_{33}$ (GV/m)	5.039	5.034	5.034	5.037	5.037	3.91/5.42	3.63/5.85
$\boldsymbol{h}_{51}$ (GV/m)	0.289	0.330	0.330	0.311	0.311	0.229/0.384	−1.92/2.67

4.2. Piezoelectric composites

4.2.1. Comparison to bounds

The predictions by the present model are compared to bounds for piezoelectric composites taken from the literature. Bisegna and Luciano (1996, 1997) derive analytical and semianalytical methods for bounding the complete set of the effective properties for continuous fiber reinforced composites, where a periodic square arrangement and square shaped fiber cross sections are assumed. Selected semianalytical results from Bisegna and Luciano (1997) for 60% volume fraction of fibers are given in Table 3, i.e. the "BL bounds" which, with the exception of $\boldsymbol{C}^D_{33}$, are the tightest among the given bounds, and the Hashin/Shtrikman-type (HS-type) bounds. The constituent material data used in Bisegna and Luciano (1997) are given in Table 1, in a form corresponding to Eq. (2).

Employing the present unit cell model, composites with circular fibers arranged in periodic hexagonal and square topologies are considered. The latter arrangement also is modeled with square fiber cross sections within the present approach, so that the edge direction of the fibers and the edge direction of the arrangement topology coincide[3]. The complete sets of the predicted overall elastic, dielectric, and piezoelectric material data for a fiber volume fraction of 60% are given in Table 3.

Direct comparison is possible for the given bounds and the values for the square shaped fiber cross section (SQE$^{\square}$) of the present unit cell approach. All results of the present model comply with both sets of bounds. Since the stiffnesses are given in terms of Eq. (7), there are piezoelectric coupling effects involved in these "elastic" values and the relation between the bounds and the unit cell results are different from the purely elastic example in the previous section.

Note that the crucial point for calculating such bounds is the choice of appropriate reference materials. Their values chosen in Bisegna and Luciano (1997) for the stiffness and piezoelectric behavior are close to the material data for the matrix and the fibers, respectively (which is in accordance to the choice for analytical HS-bounds (Hashin, 1983)). The dielectric properties of the more compliant reference material, however, deviate considerably from the data of the matrix. This is the reason for the

[3] The unit cell is modified by biasing the nodes, but keeping the mesh topology exactly the same. This way, the boundary conditions (and their implementation) remain unchanged.

(relatively) wide bounds in Bisegna and Luciano (1997) on the piezoelectric coupling moduli and on the stiffness in fiber direction, unlike in the purely elastic case.

4.2.2. Influence of fiber arrangement and fiber geometry

In addition, Table 3 shows the influence of the fiber arrangement, the fiber cross section, and the orientation of the reference coordinate system on the predicted effective material behavior. In general, the overall behavior of the composite in fiber direction is insensitive with respect to the topology. The in-plane stiffness behavior, expressed by C^D_{11}, C^D_{12}, and C^D_{66}, shows a marked dependence on orientation and arrangement. The reason for this behavior is the same as for the purely elastic case discussed in the previous section. For the fibers with square cross sections the continuous "unreinforced" regions become even more extreme and, consequently, the deviation of the material parameters is wider. The piezoelectric coupling has minor influence on this in-plane behavior because the corresponding value, $\boldsymbol{h}_{31}$, is very small.

As can be seen from Table 3 the piezoelectric and dielectric behavior of the square arrangements is invariant with respect to in-plane rotations (compare Section 2). The in-plane dielectric, $\boldsymbol{\beta}^{\varepsilon}_{11}$, and piezoelectric moduli, $\boldsymbol{h}_{31}$, as well as the out-of-plane shear piezoelectric modulus, $\boldsymbol{h}_{51}$, show a noticeable dependence on the fiber arrangement.

For a discussions on the effects of the inclusion geometry and arrangements for mechanical cases, see Shen et al. (1995), Böhm and Rammerstorfer (1995), and Weissenbek et al. (1994).

4.2.3. Poled vs. unpoled fibers

Further predictions by the present unit cell model for the square arrangement in diagonal orientation for 60% volume fraction of circular fibers are displayed in Table 4. The overall moduli are given in terms of Eq. (2), i.e. under zero electric field and zero strain, for the case of poled and unpoled piezoelectric fiber material. For the constituents in both cases the elastic data, $\boldsymbol{C}^E$, and the dielectric data, $\boldsymbol{\kappa}^{\varepsilon}$, respectively, are taken to be the same. The piezoelectric coupling is set to $\boldsymbol{e} = \boldsymbol{0}$ for the unpoled case.

The stiffness values characterizing the normal behavior of the composite, $\boldsymbol{C}^E_{11}$, $\boldsymbol{C}^E_{33}$, $\boldsymbol{C}_{12}$E, and $\boldsymbol{C}^E_{13}$, do not depend on the poling of the fibers. Overall normal strains would be suited to induce an electric field in fiber direction, but this is prevented due to the loading conditions assuming zero electric field along the continuous fibers. However, an applied electric field in this direction under zero strain gives rise to

Table 4
Predictions for the complete set of effective piezoelectric material data for square diagonal fiber arrangements for 60 vol% of poled and unpoled circular fibers ($\boldsymbol{C}^E$ and $\boldsymbol{C}^D$ denoting the elastic moduli for zero electric field and zero electric displacement, respectively)

SQD$^{\bigcirc}$	Unpoled	Poled	Poled	From Table 3
$\boldsymbol{C}^E_{11}$ (GPa)	21.584		21.616	$\boldsymbol{C}^D_{11}$
$\boldsymbol{C}^E_{33}$ (GPa)	54.595		87.100	$\boldsymbol{C}^D_{33}$
$\boldsymbol{C}^E_{12}$ (GPa)	12.298		12.330	$\boldsymbol{C}^D_{12}$
$\boldsymbol{C}^E_{13}$ (GPa)	11.855		10.839	$\boldsymbol{C}^D_{13}$
$\boldsymbol{C}^E_{44}$ (GPa)	5.996	6.679	6.696	$\boldsymbol{C}^D_{44}$
$\boldsymbol{C}^E_{66}$ (GPa)	8.216		8.216	$\boldsymbol{C}^D_{66}$
$\boldsymbol{\kappa}^{\varepsilon}_{11}$ (nC/Vm)	0.155	0.158	0.158	$1/\boldsymbol{\beta}^{\varepsilon}_{11}$
$\boldsymbol{\kappa}^{\varepsilon}_{33}$ (nC/Vm)	1.262	1.282	1.282	$1/\boldsymbol{\beta}^{\varepsilon}_{33}$
$\boldsymbol{e}_{31}$ (V/m)	0	−0.202	–	–
$\boldsymbol{e}_{33}$ (V/m)	0	6.455	–	–
$\boldsymbol{e}_{51}$ (V/m)	0	0.052	–	–

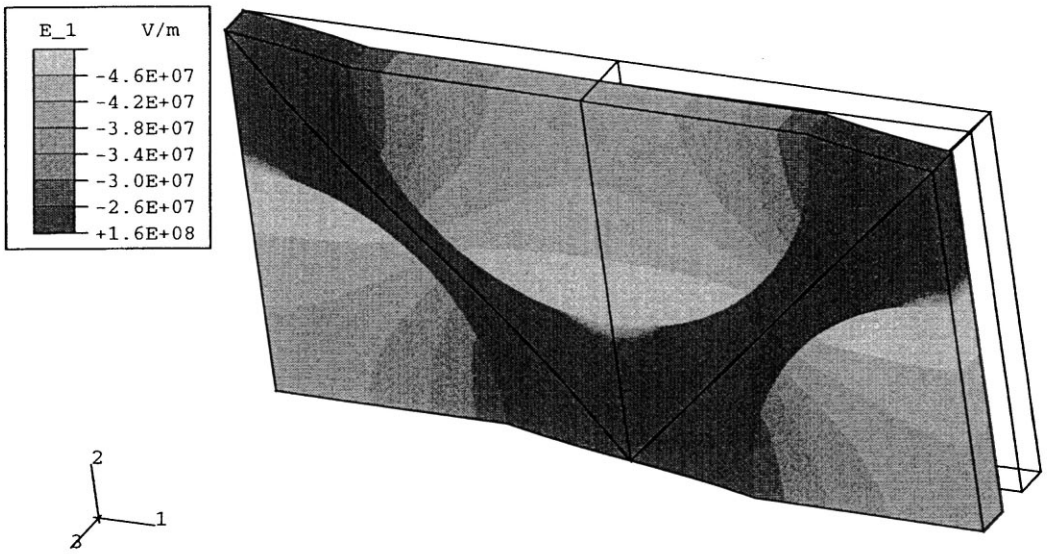

Fig. 5. Predicted local electric field E_1 under overall pure out-of-plane shear and overall zero electric field for 60 vol% of fibers in square diagonal arrangement.

different longitudinal permeabilities, $\boldsymbol{\kappa}^{\varepsilon}_{33}$, for poled and unpoled fibers. Finally, for transverse shear no coupling at all is present, neither for the fiber material nor the composites under consideration.

It is noted, that the previous considerations are made for continuous fibers belonging to the 6 mm crystal classes. Of course, materials with a lower degree of symmetry would give rise to a more complex dependence on fiber arrangement and fiber orientation.

4.2.4. Monolithic piezoelectric material vs. composite

For monolithic piezoelectric materials, the elastic response under zero electric field is equivalent to the elastic response for the unpoled material. However, this does not hold true for the fiber composites under longitudinal shear deformation, $2\varepsilon_{13}$ (and $2\varepsilon_{23}$). In that case, the piezoelectric coupling in the fibers induces a local fluctuating electric field $E_1(x)$ even though the far field is zero[4]. Fig. 5 shows this microfield under pure shear of $2\varepsilon_{13} = 0.1$. This microfield, in turn, influences the shear behavior, $\boldsymbol{C}^{E}_{44}$, of the coupled piezoelectric composite. Of course, such an interaction cannot occur in the unpoled case. For the overall dielectric behavior transverse to the fibers, $\boldsymbol{\kappa}^{\varepsilon}_{11}$, an inverse effect can be observed. Despite the fact that the overall strain is zero, local strain fields are induced in the poled fibers which affect the overall electric flux density. The overall coupling moduli in Table 4 also show some interesting features owing to piezoelectric fiber composites. The coupling moduli $\boldsymbol{e}_{31}$ and $\boldsymbol{e}_{41}$ are at least one order of magnitude lower than for the fiber material. These moduli prescribe the coupling under loading situations which are commonly referred to as matrix-dominated deformation modes. In such cases the compliant matrix accommodates almost all overall strains and the fibers experience low strains, so that the piezoelectric effect does not act in a pronounced manner. A high value is found for the overall

[4] Such considerations can be made by means of Eq. (11) applied to the local fields in the fibers.

piezoelectric modulus in the fiber direction, $\boldsymbol{e}_{33}$, because the continuous fibers are forced to carry the overall strain.

The effect of the overall behavior is also obvious, when comparing $\boldsymbol{C}^E$ to $\boldsymbol{C}^D$ (appropriate data from Table 3 are displayed again). It is noted that the latter data can also be calculated from the left hand side of Table 4. The only value which shows a marked deviation is $\boldsymbol{C}^{\times}_{33}$ which is due to the influence of $\boldsymbol{e}_{33}$.

4.2.5. Comparison with experiments

Experimentally evaluated overall material data for piezoelectric fiber composites are presented by Chan and Unsworth (1989). The constituent moduli for the PZT-7A fibers and the Araldite D matrix are given in Table 5. In order to complete the data set, additional values are taken from Dunn and Taya (1993) (marked with *). Based on the overall behavior predicted by the present model the coupling constants as given in Chan and Unsworth (1989),

$$k_t = \sqrt{1 - \frac{\boldsymbol{C}^E_{33}}{\boldsymbol{C}^D_{33}}}, \qquad k_p = \sqrt{1 - \frac{\boldsymbol{\kappa}^{\varepsilon}_{33}\boldsymbol{C}^D_{33}}{\boldsymbol{\kappa}^{\sigma}_{33}\boldsymbol{C}^E_{33}}}, \tag{17}$$

are evaluated. Fig. 6 displays these values as function of the fiber volume fraction together with the experimentally obtained results from Chan and Unsworth (1989). For the predicted values of k_p, a mild influence of the fiber arrangement (HEX or SQD) is observed for higher volume fractions. For such cases the interaction of neighboring fibers depends on the fiber spacing which is different for the arrangements considered here. The predictions for k_t are independent of the fiber arrangement within the investigated range of the volume fraction. The results predicted by the present approach are lower than the experimental values; however, Chan and Unsworth report that the nominal values of the constituents (as used in the present work) were found to deviate from the actual values. The trends shown by the experimental values are captured very well by the present model. It should be noted that the non-monotonic change of k_p with respect to the volume fraction cannot be predicted by the simpler model by Chan and Unsworth, despite the fact that only constituent properties in fiber direction are involved.

Table 5
Material data for the piezoelectric fibers (PZT-7A) and the dielectric matrix (Araldite D) after Chan and Unsworth (1989), and Dunn and Taya (1993) *)

	PZT-7A	Araldite D
$\boldsymbol{C}^E_{11}$ (GPa)	148.0	8.0
$\boldsymbol{C}^E_{33}$ (GPa)	131.0	8.0
$\boldsymbol{C}^E_{12}$ (GPa)	76.2	4.4
$\boldsymbol{C}^E_{13}$ (GPa)	74.2	4.4
$\boldsymbol{C}^E_{44}$ (GPa)	25.4 *	1.8
$\boldsymbol{C}^E_{66}$ (GPa)	35.9	1.8
$\boldsymbol{\kappa}^{\varepsilon}_{11}$ (nC/Vm)	4.065 *	0.0354
$\boldsymbol{\kappa}^{\varepsilon}_{33}$ (nC/Vm)	2.079	0.0354
$\boldsymbol{e}_{31}$ (C/m^2)	−2.1	–
$\boldsymbol{e}_{33}$ (C/m^2)	9.5	–
$\boldsymbol{e}_{51}$ (C/m^2)	9.2 *	–

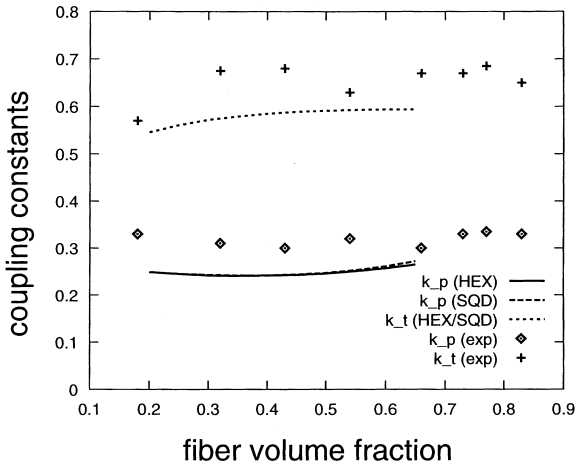

Fig. 6. Predictions of the present approach on the overall behavior of piezoelectric composites with hexagonal (HEX) and square (SQD) fiber arrangements, comparison to experimental data from Chan and Unsworth (1989); for definition of the coupling constants k_p and k_t see text.

5. Conclusions

A comprehensive unit cell model is developed for studying composites with periodic hexagonal or square arrangements of continuous fibers by means of the finite element method. The boundary conditions giving rise to consistent behavior under arbitrary mechanical and electrical loading conditions are discussed in detail and checked for the elastic and piezoelastic cases. The comprehensive unit cell model is an extension of the widely used standard models, but it relieves the restrictions of the standard models to some specific loading modes. The model can be applied to simulate any loading mode and loading path in nonlinear composites. In addition to the capability of predicting the complete set of overall composite properties, the local fields arising in response to arbitrary homogeneous overall loads can be obtained with high resolution.

In the present work piezoelectric composites are considered with a dielectric matrix material and fully coupled piezoelectric fibers. The complete set of overall moduli is predicted for various fiber arrangements and fiber cross sections. These results are compared to (semi)analytical bounds from the literature, where agreement is found for all moduli when considering identical microstructures. A marked influence of the fiber arrangement on the overall behavior is found for the elastic and dielectric properties transverse to the fibers, and the piezoelectric modulus which couples the electric field with shear deformation. The overall dielectric behavior changes depending on whether or not the fibers are poled; with respect to the elastic behavior only the longitudinal shear modulus is altered. For the composites a pronounced piezoelectric coupling effect is found only in fiber direction. The coupling transverse to the fibers is very weak due to the accommodation of transverse strains mainly in the matrix. Data for experimentally evaluated coupling constants from the literature compare satisfactory with the predictions. The dependence on the fiber volume fraction is also predicted very well.

Acknowledgements

The authors gratefully acknowledge the discussions with H.J. Böhm of the Christian Doppler

Laboratory for Functionally Oriented Materials Design at the Institute of Light Weight Structures and Aerospace Engineering, Vienna University of Technology. HP's post-doctoral study at MIT was supported by an Erwin Schrödinger Fellowship (grant J01371-TEC) from the Austrian Science Fund.

References

ABAQUS 1996. Version 5.6, User Manual. Hibbitt, Karlsson and Sorensen, Pawtucket, RI.

Adams, D.F., Crane, D.A., 1984. Finite element micromechanical analysis of a unidirectional composite including longitudinal shear. Comput. and Struct 18 (6), 1153–1165.

Anthoine, A., 1995. Derivation of the in-plane elastic characteristics of masonry through homogenization theory. Int. J. Sol. Struct 32 (2), 137–163.

Benveniste, Y., 1992. The determination of the elastic and electric fields in a piezoelectric inhomogeneity. J. Appl. Phys 72 (3), 1086–1095.

Benveniste, Y., 1993. Universal relations in piezoelectric composites with eigenstress and polarization fields. Part I: Binary media — local fields and effective behavior. J. Appl. Mech 60 (2), 265–269.

Bisegna, P., Luciano, R., 1996. Variational bounds for the overall properties of piezoelectric composites. J. Mech. Phys. Sol 44 (4), 583–602.

Bisegna, P., Luciano, R., 1997. On methods for bounding the overall properties of periodic piezoelectric fibrous composites. J. Mech. Phys. Sol 45 (8), 1329–1356.

Böhm, H.J., 1993. Numerical investigation of microplasticity effects in unidirectional longfiber reinforced metal matrix composites. Modell. Simul. Mater. Sci. Engng 1 (5), 649–671.

Böhm, H.J., Rammerstorfer, F.G., 1995. Fiber arrangement effects on the microscale stresses of continuously reinforced MMCs. In: Pyrz, R. (Ed.), Microstructure-Property Interactions in Composite Materials. Aalborg University Press, Aalborg, Denmark, pp. 51–62.

Brockenbrough, J.R., Suresh, S., 1990. Plastic deformation of continuous fiber-reinforced metal-matrix composites: effects of fiber shape and distribution. Scr. Metall. Mater 24, 325–330.

Chan, H.L.W., Unsworth, J., 1989. Simple model for piezoelectric ceramic/polymere 1–3 composites used in ultrasonic transducer applications. IEEE Trans. Ultrason. Ferroelectrics Frequency Control 36 (4), 434–441.

Chen, T., 1993. Piezoelectric properties of multiphase fibrous composites: some theoretical results. J. Mech. Phys. Sol 41 (11), 1781–1794.

Cleveringa, H.H.M., van der Giessen, E., Needleman, A., 1997. Comparison of discrete dislocations and continuum plasticity predictions for a composite material. Acta Metall. Mater 45 (8), 3163–3179.

Dunn, M.L., Taya, M., 1993. Micromechanics predictions of the effective electroelastic moduli of piezoelectric composites. Int. J. Sol. Struct 30 (2), 161–175.

Dunn, M.L., Wienecke, H.A., 1997. Inclusions and inhomogeneities in transversely isotropic piezoelectric solids. Int. J. Sol. Struct 34 (27), 3571–3582.

Dvorak, G.J., 1992. Transformation field analysis of inelastic composite materials. Proc. Roy. Soc. London A437, 311–327.

Gaudenzi, P., 1997. On the electromechanical response of active composite materials with piezoelectric inclusions. Comput. Struct 65 (2), 157–168.

Gunawardena, S.R., Jansson, S., Leckie, A., 1993. Modeling of anisotropic behavior of weakly bonded fiber reinforced MMC's. Acta Metall. Mater 41 (11), 3147–3156.

Hashin, Z., 1983. Analysis of composite materials — a survey. J. Appl. Mech 50, 481–505.

IEEE 1978. Standard on piezoelectricity, ANSI/IEEE Standard 176-1978, American National Standard Institute, New York.

Luciano, R., Sacco, E., 1997. Homogenization technique and damage model for old masonry material. Int. J. Sol. Struct 34 (24), 3191–3208.

Nakamura, T., Suresh, S., 1993. Effects of thermal residual stresses and fiber packing on deformation of metal-matrix composites. Acta Metall. Mater 41 (6), 1665–1681.

Nye, J.F., 1957. Physical Properties of Crystals, Their Representation by Tensors and Matrices. Clarendon, Oxford, UK.

Moulinec, H., Suquet, P., 1994. A fast numerical method for computing the linear and nonlinear mechanical properties of composites. C. R. Acad. Sci. Paris, série II 318, 1417–1423.

Reisner, G., Werner, E.A., Fischer, F.D., 1998. Micromechanical modeling of martesitic transformation in random microstructures. Int. J. Sol. Struct 35 (19), 2457–2473.

Shen, Y.-L., Finot, M., Needleman, A., Suresh, S., 1995. Effective plastic response to two-phase composites. Acta Metall. Mater 43 (4), 1701–1722.

Smit, R.J.M., Brekelmans, W.A.M., Meijer, H.E.H., 1998. Prediction of the mechanical behavior of nonlinear heterogeneous systems by multi-level finite element modeling. Comput. Methods Appl. Mech. Engrg 155, 181–192.

Smith, W.A., Auld, B.A., 1991. Modeling 1–3 composite piezoelectrics: thickness-mode oscillations. IEEE Trans. Ultrason. Ferroelectrics Frequency Control 38 (1), 40–47.

Suquet, P.M., 1987. Elements of homogenization for inelastic solid mechanics. In: Sanchez–Palencia, E., Zaoui, A. (Eds.), Homogenization Techniques in Composite Media. Springer-Verlag, Berlin, pp. 194–278.

Teply, J.L., Dvorak, G.J., 1988. Bounds on overall instantaneous properties of elastic-plastic composites. J. Mech. Phys. Sol 36 (1), 29–58.

Wang, B., 1992. Three-dimensional analysis of an ellipsoidal inclusion in a piezoelectric material. Int. J. Sol. Struct 29, 293–308.

Weissenbek, E., Böhm, H.J., Rammerstorfer, F.G., 1994. Micromechanical considerations of arrangement effects in particulate reinforced metal matrix composites. Comput. Mat. Sci 3 (2), 263–278.